

DEVELOPMENT AND CHARACTERIZATION OF A SOLAR-BASED ENERGY HARVESTING AND POWER MANAGEMENT SYSTEM FOR A WSN NODE APPLIED TO OPTIMIZED GOODS TRANSPORT AND STORAGE

P. Visconti * [1], R.Ferri [2], M.Pucciarelli [3#] and E.Venere [4#]

Department of Innovation Engineering, University of Salento, 73100, Lecce, Italy

[#] Company Medinok SPA, 80040 Volla, Napoli, Italy.

Emails: paolo.visconti@unisalento.it [1], roberto.ferri92@gmail.com [2],

m.pucciarelli@medinok.com[3], eugenio.venere@medinok.com[4].

Submitted: Aug. 31, 2016 ***Accepted: Oct. 19, 2016*** ***Published: Dec. 1, 2016***

Abstract – This paper describes a harvesting and power management system that can be equipped with a Wireless Sensor Network (WSN) node in order to harvest energy presents in the environment to be used for sensor node power supply. The proposed scope is to develop a harvesting board exploiting available integrated circuits and devices for extending battery life-cycle of sensor node developed by Medinok SPA. The aim is to realize a WSN able to perform a monitoring of principal physical parameters deemed of interest in a facility, as automatic as possible, for the storage and handling of goods, applied for example to a commercial seaport, where stored containers need to be continuously monitored. Battery life-time is a main problem especially in networks where sensor nodes are not easily accessible. For this reason, sensor nodes are commonly equipped with power management devices able to supply power in an intelligent way from the harvester when harvestable energy is available or from backup batteries ensuring, under every operating conditions, the correct functioning of the sensor node. In this work, a solar-based harvesting system, based on* LTC3330 IC, *was designed and tested on Medinote sensor node but usable for any device requiring to be fed.

Index terms: Harvester, Power management system, Wireless sensor network, Solar cells, Sensor node power supply, Battery life-cycle, Experimental setups for harvester characterization, Measurements.

I. INTRODUCTION

In recent years, many research activities have focused on the concepts of *Internet of Things* (IoT) and *Wireless Sensor Networks* (WSNs). The acronym *IoT* indicates body area network, personal area network or local area network wherein sensors and actuators blend seamlessly with the environment around us sharing information in order to develop and map a common operating picture (COP) [1]. IoT goal is to enable objects to be connected, anytime, anyplace, with anything exploiting the use of wireless connection and unique addressing scheme in order to create smart environments. *Smart environment* term represents the evolution of the ubiquitous concept *computing*. According to [2], there are lots of features that connect this two terms, even if they have been expressed in different historical moments. The basic idea of the ubiquitous computing is the creation of a physical world dynamically and invisibly interwoven with sensors, actuators, displays and computational elements, embedded seamlessly in the everyday objects of our lives and connected through a continuous network.

There are many application areas for the IoT; in any application context, it is possible to take advantage from the interconnection between the objects that compose the entire scenario in order to share and process data. Smart homes, buildings and environmental monitoring, personal area networks, biomedical applications are just some of the application areas that can be investigated exploiting the use of WSNs [3-5]. According to [6], sensor networking is a promising technology that facilitates monitoring of physical world using a variable number of nodes distributed in space, often randomly, to monitor and store environmental parameters; these networks are highly constrained in power, computational capabilities and memory.

One of the main problem that aroused the scientific interest is connected to the power supply of sensor nodes. WSNs trend imposes a decrease of dimensions and power consumptions of sensor nodes and, at the same time, a WSN requirement is that the life-cycle and battery life of the sensor node and of the entire networks should increase. One possible solution to the sensor node power supply that allows to increase battery life is the development of harvesting solution able to exploit the harvestable energy already present in the environments where the sensor nodes are employed to work. There are lots of harvesting techniques to derive energy from the environment; the most common energy sources are mechanical, thermal, solar, chemical and electromagnetic [7, 8]. The relative choice is function of harvestable energy availability, of the application context and sensor node required power.

This paper describes a harvesting circuital solution allowing to sustain, as much as possible, from an energy point of view the sensor node *Medimote*, the node of WSN developed by

Medinok SPA within the European project ITACA. Main goal of this project is to develop and test innovative wireless technologies ensuring goods traceability and services with regard to stored goods and containers placed in monitored areas, such as ports and airports.

Main features that a device of energy harvesting and power management should present are:

- Backup batteries in order to ensure the proper operation of the sensor node when the source of harvesting is not available for long times;
- Priority control on the power supply to be used at a given instant (in order to exploit harvester system or backup batteries);
- Supercapacitor or ultracapacitor charging in order to store energy when the harvestable energy is greater than the required from the sensor node.

Before defining and developing the energy harvesting and power management device for low-power WSNs, it is necessary to analyze in depth the basic elements of ITACA project WSN. Determining the magnitude of energy consumption of the sensor node, it will be possible to choose, among the various types of adoptable harvesters, the better solution able to supply the Medimote sensor node and to make it energetically autonomous, as much as possible.

II. ITACA WSN FOR GOODS TRANSPORT AND STORAGE: BLOCK DIAGRAM AND FUNCTIONALITIES OF DESIGNED MEDIMOTE SENSOR NODE

The basic element of a WSN is represented by the sensor node; its architecture can be more or less complex depending on application context and number of variables to be monitored. In addition to sensing functionality, nodes must have processing and management capabilities of collected data. Hardware of a sensor node generally includes the following parts: the power supply and management module, some on board sensors, a microcontroller unit, memory storage units and a wireless transceiver. The microcontroller is the main system as it handles the data received from sensors and manages actuators. Microcontrollers also have the task of optimizing sensor nodes from an energy point of view: exploiting its capabilities, it is possible to put on board sensors or other parts of HW in low power mode. Supercapacitors are well suited to be integrated within sensor nodes and are often associated with energy harvesting system to ensure, under certain conditions, sensor node operation without involving backup batteries. A general node architecture with all its parts is shown in figure 1.

The challenge in WSNs field is to provide high-performances sensor node self-maintained in terms of energy and possibly low cost. Thus, different energy sources were employed to store an energy quantity to make sensor node energetically self-sufficient in its entire life-cycle.

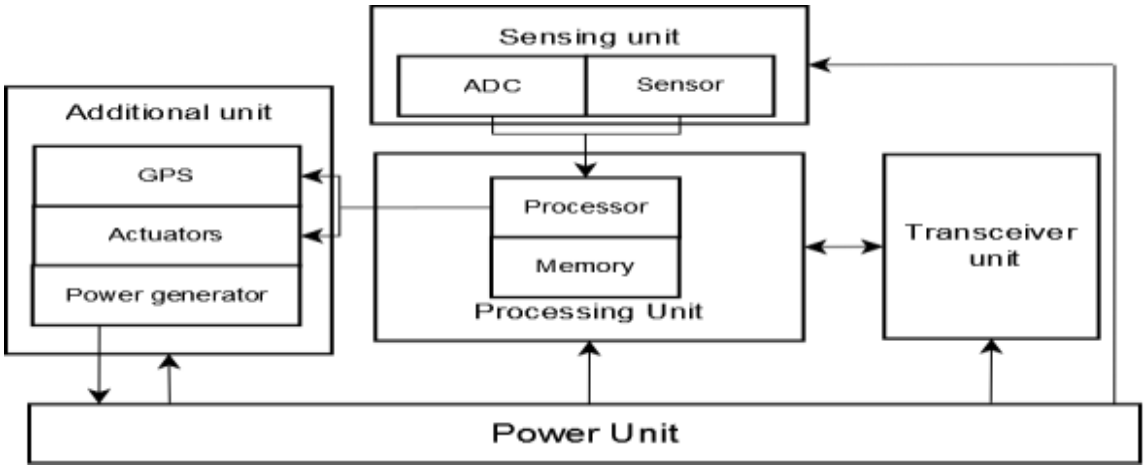


Figure 1. Typical hardware architecture of a wireless sensor node

The harvesting device generally provides a small amount of energy and for this reason multiple devices afferent to different energy sources are often used. Through this approach, it is possible to store energy within storage devices such as batteries or supercapacitors to be used later for example during transmission operations. In fact, the higher energy consumption occurs during the transmission of data which involves the use of the RF module.

Sensor node operation, in most of application contexts, is characterized by long periods of inactivity compared to required time to send the information detected by sensors. Thus, the use of energy storage devices together with harvesting systems is fundamental to store energy during inactivity time using the available energy sources in the environment.

According to [9], the continuing development of WSNs and their flexibility extend the application contexts that can be examined using sensor nodes. Developed harvesting system described in this paper has been optimized and characterized for *Medimote* sensor node with the aim to reduce utilization of the batteries supplying sensor node. The project purpose is the creation of a logistics management system based on the use of innovative WSN in order to reduce the need of human intervention. The application context is shown in figures 2 and 3.

The sensor node has the purpose of monitoring some quantities related to the environment in which the container is inserted and to send them to control center exploiting local gateways. Developed energy harvesting system must allow the sensor node to carry out all required operations; moreover the power management module must guarantee correct operation of the sensor node in every condition. For this reason, two different power supplies are used, the first associated to the harvester and the other, like backup battery, to support the node when no power is available from harvesting block. Figure 4 shows the block diagram of sensor node including the processing unit, the wireless module, a storage unit, some on board sensors and digital and analog external sensors inputs.

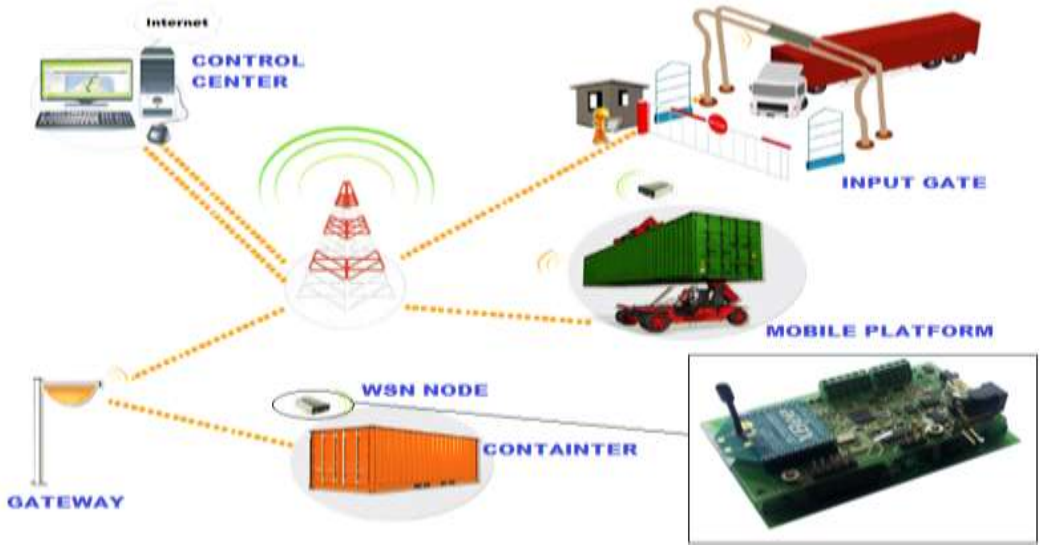


Figure 2. Graphical representation of a typical scenario with reference to the ITACA project



Figure 3. ITACA WSN applied to stored containers for goods monitoring

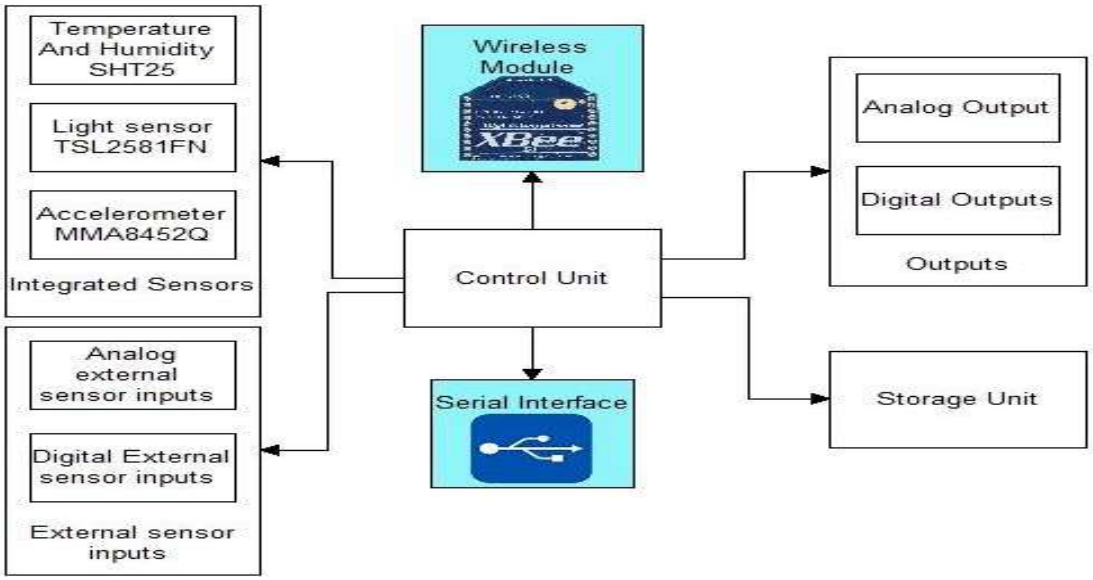


Figure 4. Block diagram of the designed and realized Medimote sensor node

The processing unit is provided with Microchip PIC24F32KA302 16-bit microcontroller with extreme low-power consumption specially designed for battery powered systems/applications. The data storage unit is a EEPROM Microchip 24LC1026 chip, a 1024 Kbit electrically erasable PROM capable of operation across a broad voltage range. As regards on board sensors, the Sensirion SHT25 device is provided for temperature and humidity measurements, based on a capacitive type humidity sensor and a band gap temperature sensor. A light sensor is also present, the Taos TSL2581FN device, with a very-high sensitivity light-to-digital converter that transforms light intensity to digital output signal with I^2C interface. Finally, the *Medimote* sensor node has embedded a MMA8452Q accelerometer, a smart low-power, three-axis, capacitive, micro-machined accelerometer with 12 bits of resolution. Figure 5 shows a photograph of *Medimote* board with the main elements that compose sensor node highlighted.



Figure 5. Hardware view of the principal components of Medimote sensor node

The wireless module chosen for communication between sensor nodes is Digi International XBee XB24 device, with a working frequency of 2.4GHz, a data rate of 250kbps using a direct sequence spread spectrum modulation. The component is critical with reference to power consumption, being the component that most of all requires power, specially in the data transmission phase. Table 1 shows the technical features of XBee and XBee Pro modules.

XBee	
Indoor/Urban range:	up to 30m
Outdoor line-of-sight:	up to 90m
TX Peak Current:	45 mA (3.3V)
RX Current:	50mA (3.3V)
XBee Pro	
Indoor/Urban:	up to 90m
Outdoor line-of-sight:	up to 1600m
TX Peak Current:	250 mA (3.3V)
RX Current:	340mA (3.3V)

Table 1. Xbee module Features: XBee and XBee Pro comparison.

XBee-Pro module allows to cover larger areas than the basic one at the expense of significantly higher power consumption; this aspect would make difficult the implementation of circuits able to render autonomous, from the energy point of view, the sensor node.

According to [10] and [11], one popular mesh networking protocol is ZigBee, a low-cost low-power, wireless mesh network standard targeted at the wide development of long battery life devices in wireless control and monitoring applications. ZigBee protocol defines three type of nodes: coordinator, router and end device. All nodes can send and receive data but there are differences in the specific role they play into the network; coordinators are the most capable of the three node types. There is one coordinator in each network able to store information about network including security keys. Routers act as intermediate nodes, relaying data from other devices like end devices or sensor nodes; end devices can be low-power/battery-powered devices.

Additionally to ZigBee protocol, there is a recent alternative mesh protocol named Digi-Mesh; unlike Zigbee, this kind of protocol has only one node type, all nodes can route data, can be configured as low-power/battery-powered devices, are interchangeable and there are no parent-child relationships. Another feature of DigiMesh protocol is the possibility to put in sleep mode all sensor nodes allowing to increase battery lifetime. So, sensor nodes alternate sleep and wake-up periods managing their sleep schedule to make feasible and efficient communication. As explained in [12], the design of efficient duty-cycling schemes is not straightforward; with reference to ITACA project, in order to develop and test the realized harvesting device, the node is activated only for 10 seconds while it remains in sleep mode for the other 50 seconds for each one-minute cycle so reducing significantly power consumption.

III. CONSUMPTION ANALYSES OF THE MEDIMOTE SENSOR NODE

First step to reduce sensor node power consumption is to set the transmission module in sleep mode during sensors interrogation and data storage, especially helpful for battery powered nodes. In fact, component that most of all requires power when sensor node is active is XBee module and thus it is necessary to activate RF module only when data transmission or reception is required. Figure 6 shows the experimental setup for sensor node consumption monitoring. By using a 10Ω high precision resistor, connected in series with the sensor node, and detecting voltage drop across the test resistor, current absorbed from node during activation and sleep phases is obtained. The described experimental tests were carried out for all the three versions of *Medimote* sensor node (shown in figure 7).

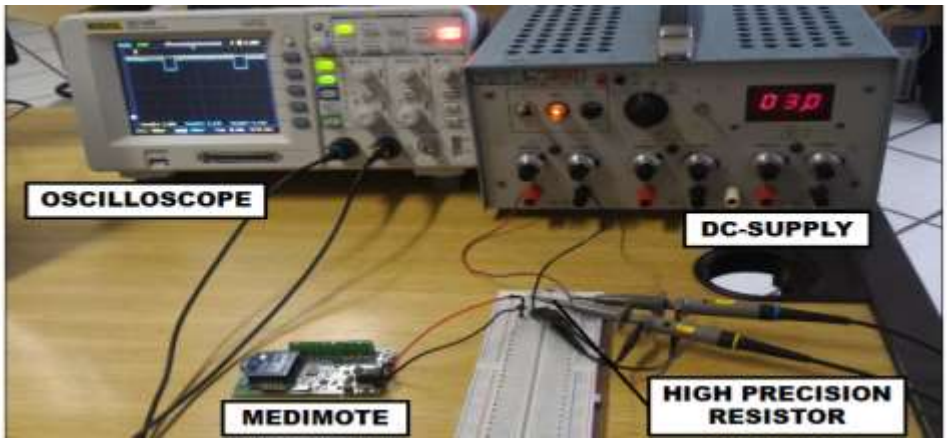


Figure 6. Experimental setup for consumption measurement of the sensor node

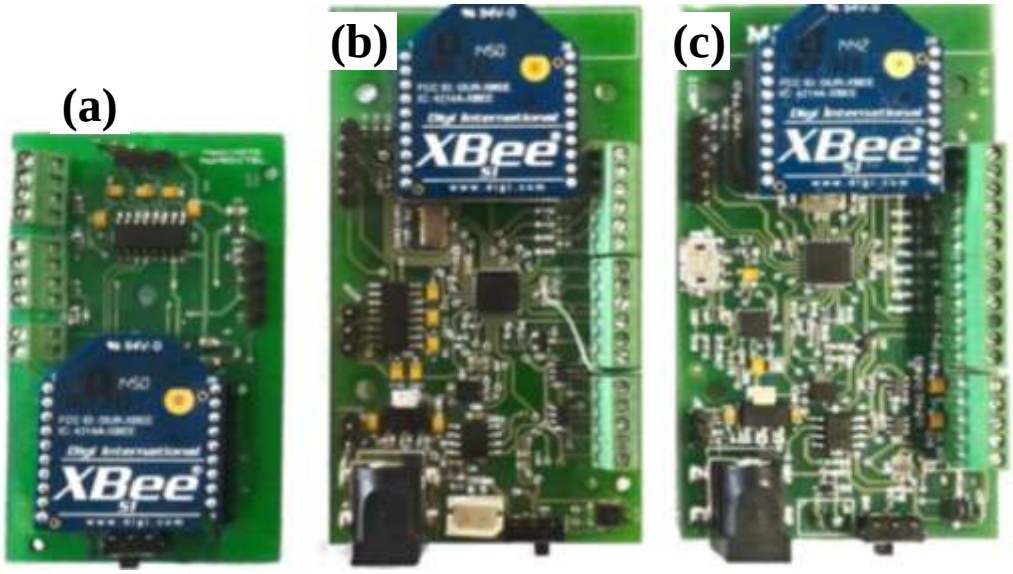


Figure 7. Hardware evolution of three different prototypes of Medimote sensor node in chronological order: Medimote 1.0 (a), Medimote 2.0 (b), Medimote 3.0 (c)

In figure 8, time behaviour of voltages before and after test resistor is shown; voltage from the DC-supply (blue colour) is set to 3V (operating voltage of sensor node) whereas the voltage applied to the sensor node (after test resistor) is plotted in red colour.

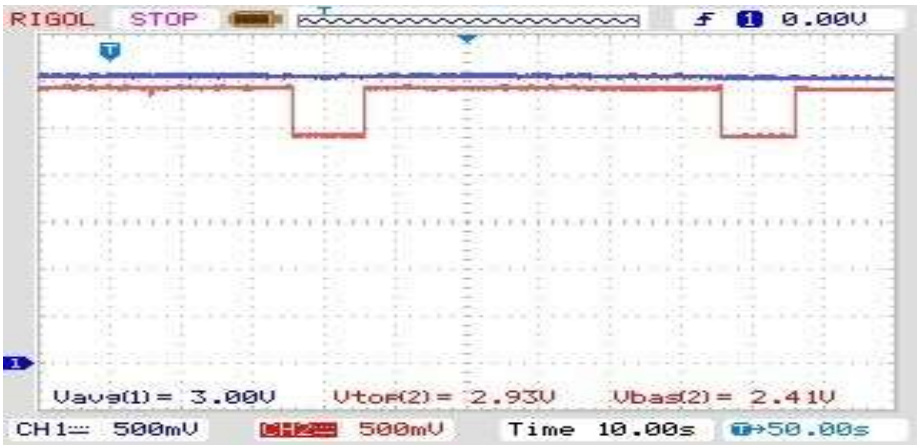


Figure 8. Voltage before the test resistor (blue colour) set at 3V by the DC-supply and, with red colour, voltage downstream of the test resistor during activation and sleep phases

Medimote 3.0 node can work even with supply voltage lower than 3V (up to 2.4V) and for this reason, the voltage drop on test resistor does not afflict its operation. Consumption measurements were conducted for all Medimote versions to find the order of magnitude of required power; afterwards, only consumption analysis for Medimote 3.0 device is reported. Current absorbed by the sensor node during operating cycle is characterized by a maximum value I_{max} (with sensor node active) and a minimum value I_{min} during sleep phase.

$$I_{max} = \frac{V_{avg} - V_{bas}}{R_{test}} = \frac{3.00 - 2.41}{10} \simeq 59mA$$

$$I_{min} = \frac{V_{avg} - V_{top}}{R_{test}} = \frac{3.00 - 2.93}{10} \simeq 7mA$$

and then follows that:

$$P_{transm} = V_s \cdot I_{max} = 3 \cdot 59 \cdot 10^{-3} = 177mW$$

$$P_{sleep} = V_s \cdot I_{min} = 3 \cdot 7 \cdot 10^{-3} = 21mW$$

Carried out analysis represents the base for choice of the harvesting system capable to store in the accumulation device a sufficient amount of energy for sensor node feeding. Knowing order of magnitude of node power consumption, the choice between harvester types becomes easier in order to guarantee sufficient autonomy in terms of energy to the sensor node.

IV. SOLAR POWER GENERATION FOR ENERGY HARVESTING SYSTEMS

The possibility to make a sensor node completely autonomous in terms of energy depends on several factors including its hardware complexity. A block diagram of an energy autonomous system (EAS) is reported in figure 9 [13]; its structure can be divided in 3 parts:

- Energy generation: this section consists of energy sources and harvesting unit. Usually harvesting section is composed of more elements related to various types of sources.
- Energy conversion and optimization: conversion of energy provided by the harvesting section is a main function of EAS in order to maximize the efficiency of entire system;
- Energy consumption: this section is composed of the sensor node or in general from devices which use energy stored in the accumulation units. The possible integration of energy harvesting system strongly depends on efficiency of this section [14].

In literature, there are several works that allow to get an overview on the various harvesting systems. In [15] and [16], a comparison in terms of available output power for different available harvesting techniques is discussed and summarized. This analysis combined with *Medimote* consumption allows to have all needed information for harvesting system choice.

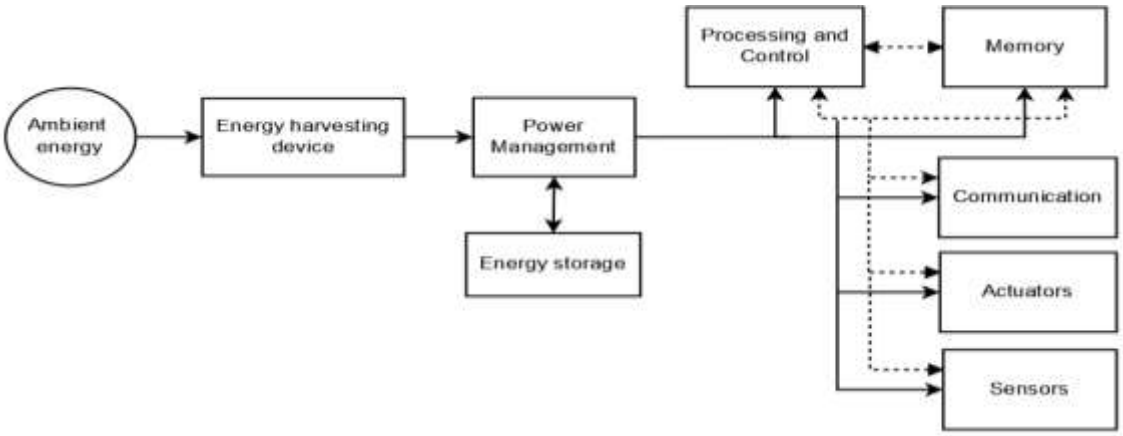


Figure 9. Block diagram of a low-power energy autonomous system

A strategy adopted in application contexts in which it is possible to recover energy from more types of sources, is the design of a hybrid power source to obtain required power and to guarantee sensor node functionalities. In [14] and [15], it is highlighted that power consumed by a network node can be split between the various functions that it has to perform. Power requirements of each section of a sensor node depends on particular application and it is difficult to state which consumes more power without performing a consumption analysis. Energy amount recoverable from a single harvester is typically small and variable with time, location and working conditions. *Medimote* node consumption is rather high and application context narrows the types of harvester that can be used. The harvesting solution more suitable to be implemented is that based on the solar cells, able to provide enough power even with cell areas of a few cm^2. According to [17], mote lifetime can be increased more efficiently by solar-based harvesting techniques rather than other sources available in outdoor scenarios.

The I/V and power-voltage curves of a solar cell are shown in figure 10 for different irradiation conditions. According to [18], maximum power point (MPP) tracking has to be used to maximize the power extraction finding, in any time of the day, I_{MPP} current and V_{MPP} voltage for getting maximum product $I_{MPP} * V_{MPP}$value. Due to variability of solar cell output power as function of sunshine intensity and ambient temperature, MPP tracking systems are often associated with energy harvesting devices, in order to constantly track the MPP that a source is capable of delivering depending on boundary and operating conditions.

Figure 11 shows a block diagram of a solar cells-based harvesting system applied to WSN node. Some commercial solar cells are very compact and permit to get sufficient energy to feed sensor nodes that require high power during normal operation. Figure 12 shows a commercial solar cell and in the table its physical and electrical features. The decision to use small solar cells is also justified by the fact that containers, once entered the port zone, are placed in outdoor area assigned by the control center, so they are subject to solar radiation.

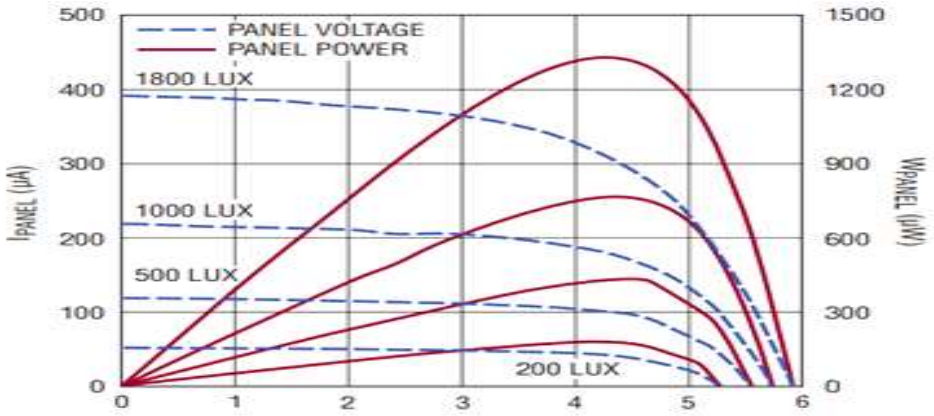


Figure 10. Output current-voltage and power-voltage characteristic curves of a solar cell for different irradiation conditions

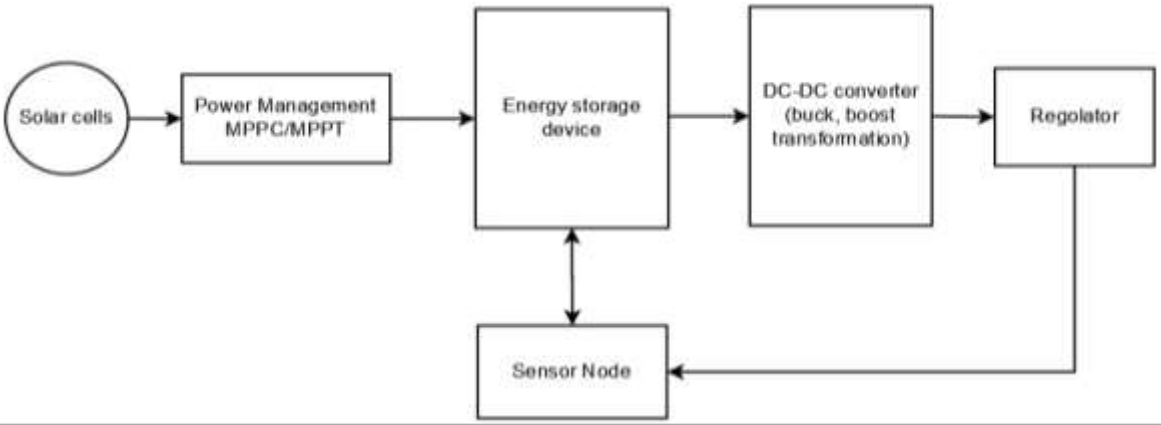
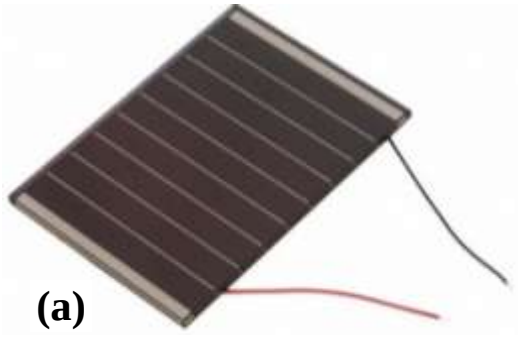


Figure 11. Block diagram of solar energy harvesting system for low power WSN application



Power Max	229mW
Current Pmpp	45.7mA
Voltage Pmpp	5V
Current Short Circuit	22.3mA
Type	Amorphous
Voltage-Open Circuit	7.7V
Dimension	75.0 mm x 55.0 mm x 2.3 mm

(b)

Figure 12. Panasonic BSG AM-5907CAR solar cell (a) and its physical and electrical features

V. DESIGN AND TESTING OF A HARVESTING AND POWER MANAGEMENT SYSTEM FOR MEDIMOTE SENSOR NODE

After choosing energy harvesting source, some ICs for the power management block were analysed. The IC that more than others presents suitable characteristics is the nano-power LTC3330 buck-boost DC/DC converter with battery life extender, allowing us to design a harvesting board easily adaptable to other WSN nodes. The LTC3330 is a Linear Technology IC with important characteristics for energy harvesting and WSNs applications; it is available in a 5mm x 5mm QFN-32 package and thus easily applicable to small devices such as sensor

nodes. LTC3330 integrates a high voltage energy harvesting power supply plus a DC/DC converter powered by a primary cell battery to create a single output supply for alternative energy application.

The energy harvesting power supply, consisting of an integrated full-wave bridge rectifier and a high voltage buck converter, allows to harvest energy from piezoelectric, solar, or magnetic sources; moreover, either side of the bridge can operate independently as a single ended AC or DC input. LTC3330 combines a buck switching and a buck-boost switching regulator to produce an energy harvesting solution: the buck operates when harvested energy is available, reducing quiescent current draw on the battery to essentially zero, thereby extending battery life. The buck-boost powers V_{OUT} only when harvested energy goes away. The converters are controlled by a prioritizer that selects which converter to use based on availability of a battery and/or harvestable energy. The input prioritizer on LTC3330 decides whether to use energy harvesting input V_{IN} or battery input (BAT) to power V_{OUT} performing a control on harvestable energy availability. A digital output EH_{ON} can be used to understand if sensor node power supply is given by backup batteries or harvestable energy. This pin is low when the prioritizer decide to select the BAT input and is high when prioritizer selects V_{IN} input.

An important feature of LTC3330 is the buck under-voltage lockout (UVLO) implementation and its programmable thresholds. When V_{IN} voltage rises above UVLO rising threshold, buck converter is enabled and charge is transferred from input to output capacitor. UVLO thresholds are chosen depending on input source characteristics using UVLO Select Bits UV_3, UV_2, UV_1 and UV_0. Finally LTC3330 was chosen being particularly suitable for wireless systems which consume low average power but occasionally need a high burst of power to accomplish a task.

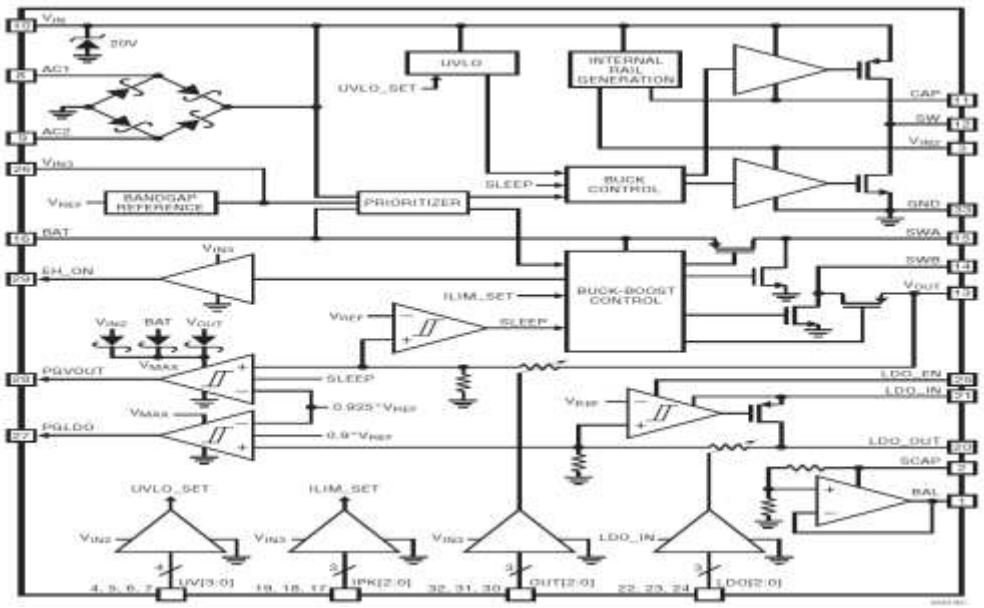


Figure 13. Internal LTC3330 block diagram

On the market, a demonstration circuit based on LTC3330 IC is available, the demo-board DC2048A (shown in figure 14); it is fundamental to test and fully learn all LTC3330 features and allows to have the related circuital schemes and the bill of needed components.

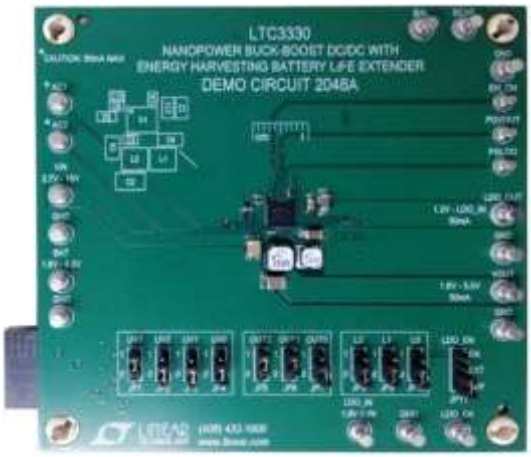


Figure 14. Demo Circuit 2048A: Nano-power Buck-Boost DC/DC converter with Energy Harvesting Battery Life Extender based on LTC3330 IC.

Before designing an energy harvesting prototype based on LTC3330 IC, it was decided to use the measurement setup shown in figure 15 to investigate principal LTC3330 characteristics.

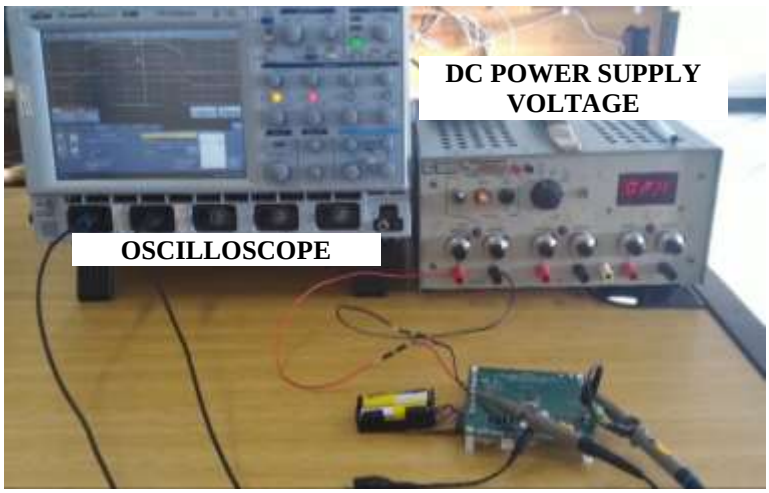


Figure 15. Measurement setup used to monitor the voltage levels of the principal DC2048 pins

In figure 16, the trends of input (Vin) and output (Vout) voltages of the DC2048A demo circuit are shown, during simulation of the harvester shutdown. Vout is set at 3V equal to the sensor node operating voltage exploiting related output selecting jumpers. Vout remains constant at 3V even if harvester stops working or V_{IN} pin voltage drops under UVLO falling threshold: a backup battery ensures the desired level of output voltage Vout. When harvestable energy is available, it is transferred through bridge rectifier and accumulated on the input capacitor, powering the sensor node. The need to have a stable Vout voltage of LTC3330 is related to node power supply which has to be as stable as possible to prevent *Medimote* malfunctions.

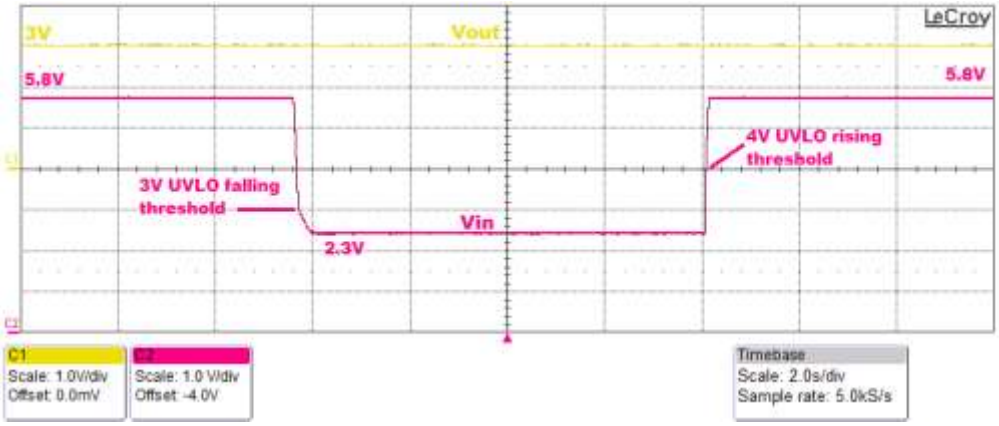


Figure 16. Harvester Shutdown Simulation: LTC3330 Vout set to 3V (yellow colour) and the DC-supply output voltage connected to the LTC3330 V_{IN} pin (purple colour).

In figure 17, EH_{ON} pin behaviour is shown when conditions on pins AC1, AC2 or V_{IN} change. When AC1 input is connected to the DC-supply voltage and it is greater than 4V (selected UVLO rising threshold), prioritizer chooses to power the sensor node using the harvestable energy (simulated by DC power supply); when the DC-supply voltage falls below 3V, node feeding is supplied through the backup battery and the EH_{ON} pin goes to the low logic level.

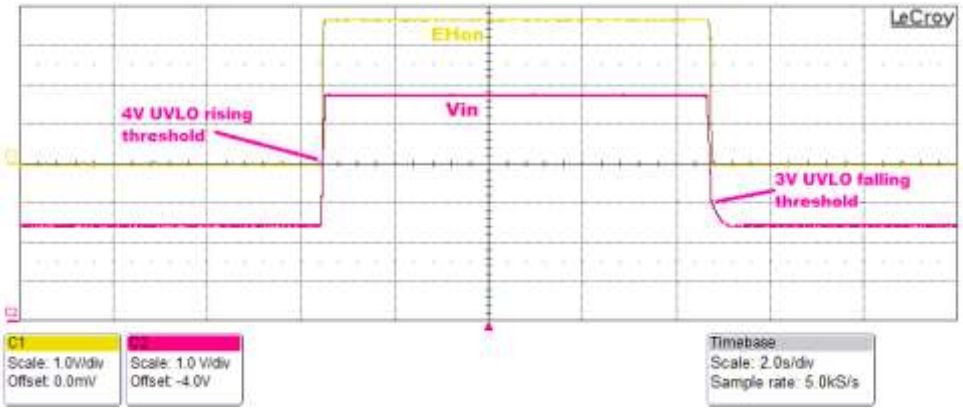


Figure 17. Harvester Shutdown EH_{ON} pin monitoring: LTC3330 EH_{ON} voltage (yellow colour) and the DC-supply output voltage connected to LTC3330 V_{IN} pin (purple colour)

a. DESIGN AND TESTING OF HARVESTING SOLUTION FOR THE MEDIMOTE POWER SUPPLY

On the basis of DC2048A demo-board tests, a powerful solution for the scenario under consideration could be identified; by using LTC3330 IC, a complete circuit was defined, able to ensure the following properties:

- Maximum power point control based on buck under-voltage lockout UVLO;
- Supercapacitor charging when more harvesting energy is available respect to the required one by the *Medimote* sensor node;
- Priority control using LTC3330 internal prioritizer for sensor node power supply (harvester or backup battery);

- Backup battery to ensure the proper operation of the sensor node during the start-up phase of the device or during long periods of unavailability of the harvesting energy;
- Regulated DC-DC output voltage.

The harvesting solution shown in figure 18 has been obtained exploiting the DC2048A Demo-Circuit; solar cells selected for the harvesting section (Panasonic BSG AM-5907CAR model) were previously described and present I_{MPP} = 45,7mA and V_{MPP} = 5V. Their choice was determined from DC2048A demo-circuit input characteristics and from their physical dimensions comparable to the *Medimote* sensor node.

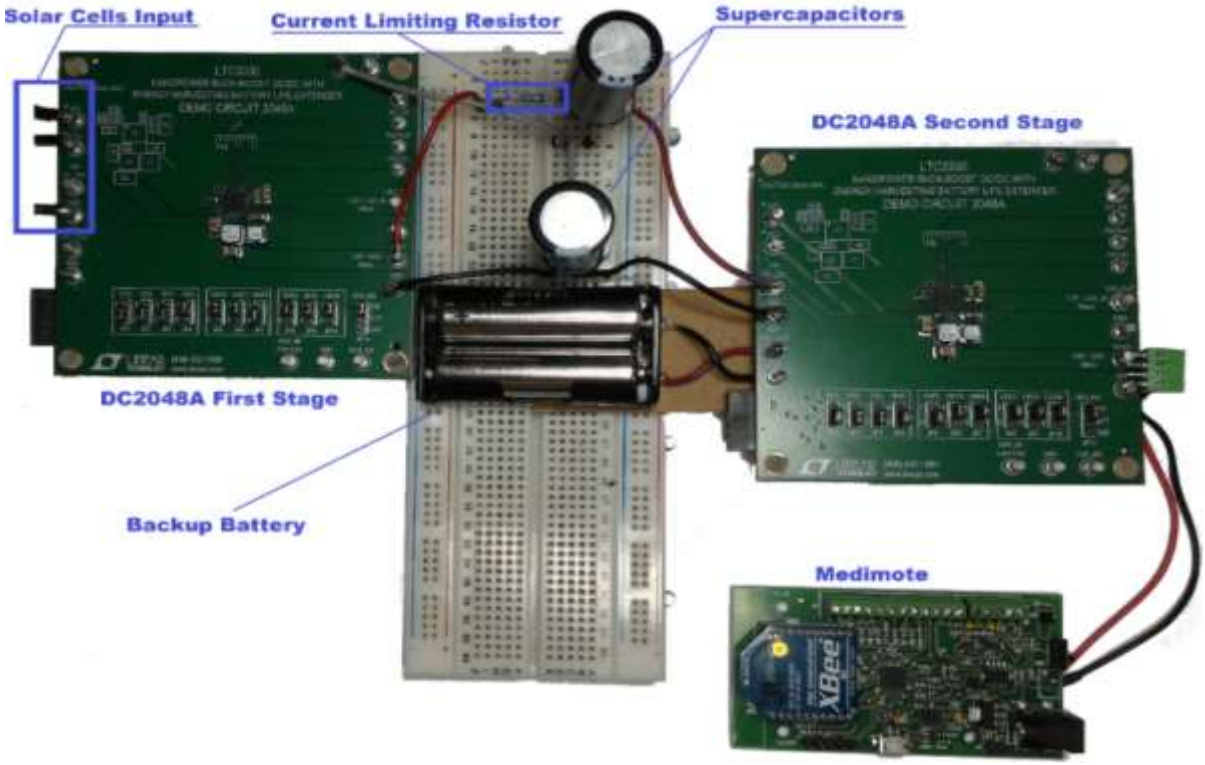


Figure 18. Harvesting circuit prototype for low-power sensor node composed of two DC2048A stages, a supercapacitor module, backup batteries and Medimote sensor node.

First block is composed by the DC2048A demo-circuit and allows to set, through UVLO window, working point of solar cells by performing a control on MPP transfer; UV3, UV2, UV1 and UV0 pins are set to low logic level except UV0 to have the rising UVLO threshold equal to 5V and UVLO falling threshold equal to 4V. In this way, the buck under-voltage lockout controls MPP transfer so that solar cells always work in proximity of maximum energy extraction point. If there is not enough energy availability, cells will be forced to work in the proximity of MPP that, with variable radiation conditions and considering bridge rectifier voltage drop, remains around 5V. First block output is connected to two 30F super-capacitors (connected in series due to maximum voltage that can be applied on each one); in

this way, energy provided by solar cells will not only power WSN node but, in case of strong solar energy availability, supercapacitors will be recharged creating a fall-back energy supply. This approach helps to reduce backup batteries use even on days with discontinuous availability of the harvestable energy.

First stage DC2048A output voltage is fixed through pins OUT2, OUT1 and OUT0 set to 110 respectively to have an output voltage of 4.5V. The LTC3330 DC/DC converter allows to set the second block output voltage, composed by another DC2048A, at 3V exactly the sensor node operating voltage. Second stage LTC3330 UVLO is used in an atypical manner compared to before; it is not used to monitor the harvester MPP transfer but its thresholds are exploited to enable the harvesting chain in place of backup batteries. Second stage UVLO thresholds are respectively set to 3V (falling threshold) and 4V (rising threshold) by setting UV3, UV2, UV1 and UV0 bits all to zero; so when supercapacitor charging voltage exceeds 4V, prioritizer carries out a comparison between backup batteries voltage and super-capacitor voltage applied to V_{IN} pin of second DC2048A block, thus enabling the harvesting branch.

Energy stored within supercapacitors will be exploited until related voltage across capacitor decreases to 3V (UVLO falling threshold); prioritizer is aware that supercapacitors are discharging and will rehabilitate backup batteries. The supercapacitors will never discharge below 3V because, when backup batteries are activated, circuit upstream of the last DC2048A stage is disconnected; when solar cells energy becomes again available, it will be necessary to charge supercapacitors again to 4V to enable the harvesting chain. In addition, if solar energy is available for long time periods and supercapacitors are completely charge at 4.5V, energy in excess will be used to directly feed sensor node while the capacitors remain charged to 4.5V (output voltage of first DC2048A stage). The current limiting resistor (properly sized to 10Ω after performed tests with different resistance values), shown in figure 18 and placed before capacitors, is used to avoid great instantaneous stresses for DC/DC converter output and damages to the first DC2048A stage and to the LTC3330 IC placed on board.

b. CIRCUIT ANALYSIS AND CHARACTERIZATION OF DEVELOPED HARVESTING SOLUTION

First carried out test involves the use of DC power supply (current limit set to 40mA) upstream the harvesting circuit and Medimote node connected to the prototype output; the purpose is to verify voltage values set by the jumpers on the two DC2048A demo-boards. The Medimote device has similar settings as outlined previously for consumption analysis with an operating cycle of one-minute consisting of 10 seconds of activation/transmission phase and 50 seconds of sleep phase. Figure 19 shows the measurement setup used for these tests.

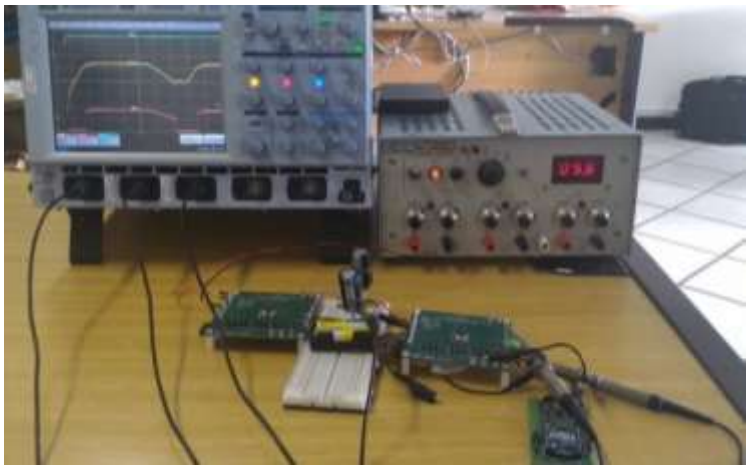


Figure 19. Experimental setup for the second prototype test: DC power supply in input and the Medimote sensor node in output.

In figure 20, three different traces are reported: in blue, the output voltage of the second stage, in yellow the voltage across the super-capacitors and in purple the EH_{ON} pin voltage.

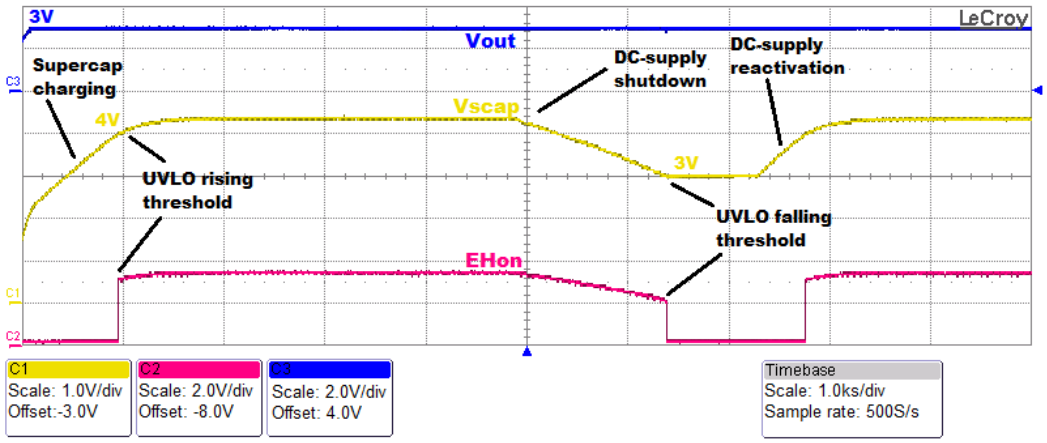


Figure 20. Output voltage measured before Medimote node (blue colour), supercapacitors voltage during DC-supply functioning and shutdown (in yellow) and EH_{ON} voltage in purple.

When there is energy availability from the harvester, this energy is stored into super-capacitors connected to the first stage output; if the voltage across super-capacitors exceeds the rising UVLO threshold (4V), the second DC2048A stage decides to supply the *Medimote* node with energy stored into super-capacitors and V_{SCAP} trace slope changes considerably. If solar cells provide enough energy to charge supercapacitors up to a voltage equal to 4.5V, then supercapacitors will appear as open circuit and a direct connection between solar cells and sensor node is established. On the contrary, if solar cells are unable to provide sufficient energy to sustain node energy consumption, the capacitors voltage begins to decrease until it reaches UVLO falling threshold (3V) and the LTC3330 prioritizer of the second stage will decide to feed sensor node through backup batteries. In this test, supercapacitors are charged

up to 4.5V through the DC power-supply; then this last is turned off in order to simulate the absence of harvestable energy, causing supercapacitors discharging (V_{scap} from 4.5V to 3V). When supercapacitors voltage exceeds UVLO rising threshold, EH_{ON} pin voltage becomes high ensuring that node power supply is given by stored energy into the supercapacitors.

Once verified the proper prototype behaviour and thresholds setting, the solar cells were connected to AC_1 and AC_2 inputs of LTC3330 first stage; realized setup is shown in figure 21.

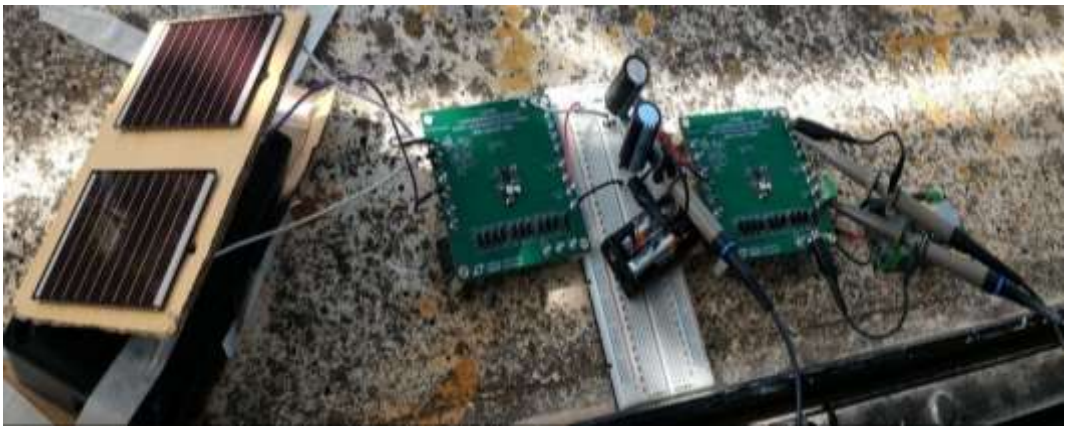


Figure 21 Experimental setup for prototype testing with solar cells applied to AC_1 and AC_2 pins of the first LTC3330 IC.

In figure 22, the UVLO behaviour is shown: during super-capacitors charging phase, voltage across solar cells is maintained around 5V (MPP voltage). When supercapacitors are charged at 4.5V, the voltage across the solar cells is brought around 7,7V or near the V_{OC}; in fact, when supercapacitors are fully charged, only power needed to the sensor node operations is required. After, if power availability of the cells significantly reduces, the UVLO returns to force cells to work around the point of maximum power transfer. After three thousand seconds, it was decided to almost completely cover the cells for verifying UVLO operation and cells operating point moves near the MPP in order to store as much harvestable energy as possible to compensate supercapacitors discharge.

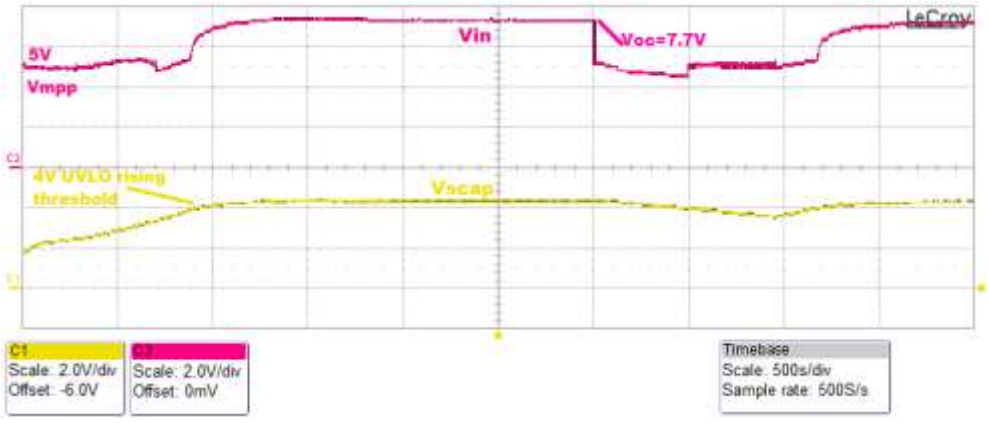


Figure 22. In red voltage from solar cell (AC_1 or AC_2 pin), in yellow supercapacitor voltage

In figure 23, Vout output voltage, voltage across supercapacitors Vscap and voltage on EH_{ON} pin, during a day with low or medium solar radiation level, are shown. Firstly, the sensor node supply voltage, after a short start-up phase, remains constant to 3V and the node is able to perform required operations. Supercapacitors charging time is very short because the two solar cells are able to deliver much more power than the DC power-supply previously used. Entire analysis has a duration of 2 hours and 45 minutes and, except in the initial phase, *Medimote* node is ever powered by the solar cells and supercapacitors are completely charged at 4.5V.

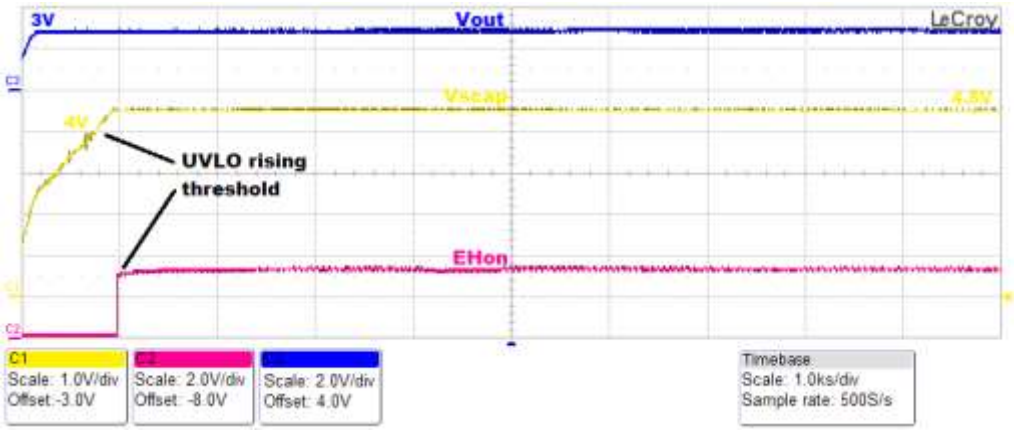


Figure 23. With blue colour, output voltage (3V) before the Medimote node, in yellow colour the supercapacitors voltage and in purple, EH_{ON} trend with low/medium solar radiation level.

Figure 24 shows that when the system is subject to lighting conditions that do not allow to derive sufficient energy from the solar cells (rainy weather or late afternoon), the voltage across the supercapacitors never reaches 4.5V value. In the test of figure 24, solar cells were completely covered and then uncovered in order to charge supercapacitors, observing what happens when solar radiation level is greatly reduced (e.g evening hours).

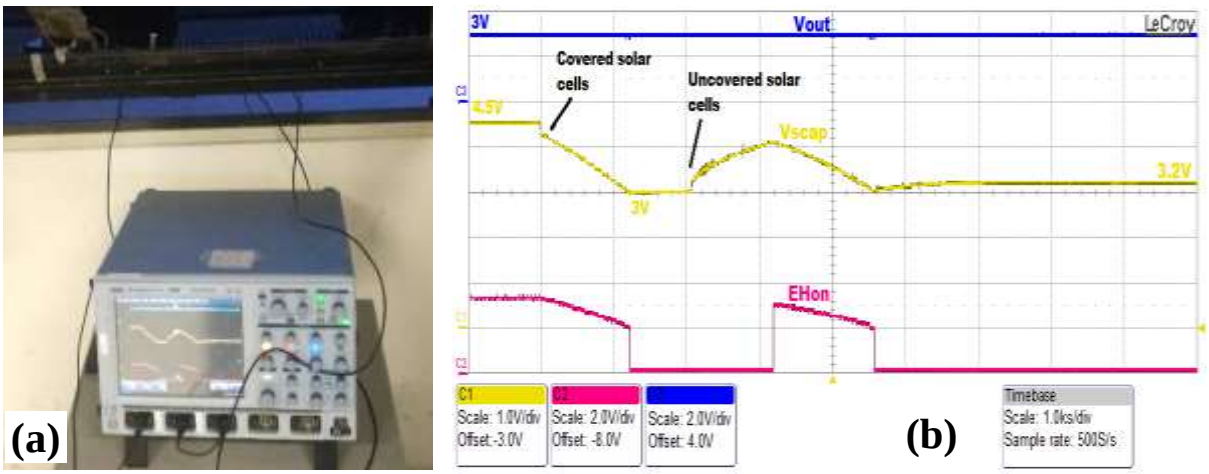


Figure 24. Experimental setup (a) and oscilloscope graph (b) in late afternoon: in blue, output voltage before Medimote, in yellow supercapacitors voltage and in purple EH_{ON} trend.

After passing UVLO rising threshold (4V), the system enables the harvester branch and consequently supercapacitors energy is used to feed the sensor node; then if it is not possible to extract enough solar energy to sustain node consumptions, supercapacitor voltage decreases up to 3V with a discharge slope related to energy provided by solar cells. Until cells ensure supercapacitor voltage over 3V, harvester is used for a variable period of time in relation to harvestable energy availability: EH_{ON} voltage is high until Vscap does not decrease below 3V. In late afternoon, charging phase is so slow that prototype is not able to keep Vscap over 3V and thus sensor node functionalities are guaranteed by using backup batteries.

In figure 25, the discharge time is determined with node activity time of 10sec and one minute cycle; the supercapacitors are charged up to 4.5V by using solar cells, then these last are completely covered in order to find out discharge phase duration with complete absence of harvestable energy. The device keeps supplying the sensor node for about 25 minutes exploiting only energy within the supercapacitors; then voltage across *Medimote* node reaches 3V and LTC3330 IC ensures stability of Vout voltage using the backup batteries.

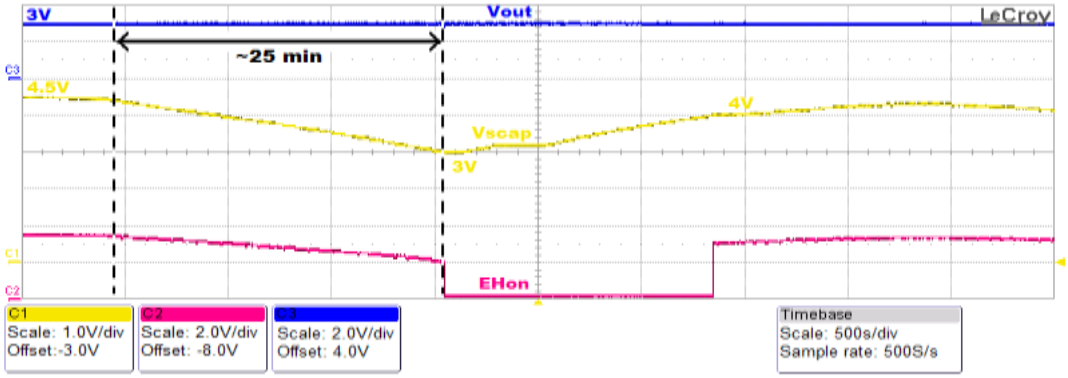


Figure 25. Supercapacitors discharge phase with node activity time of 10sec and 1min cycle.

VI. PCB DESIGN, TEST AND CHARACTERIZATION OF THE HARVESTING AND POWER MANAGEMENT BOARD

The circuit diagram and layout of developed harvesting board were implemented by using the CAD PCB software Eagle; the developed circuital solution integrates three blocks discussed in previous section, the two DC2048A stages and intermediate block consisting of two supercapacitors connected in series with value each of 30F so getting a total capacitance of 15F. PCB layout was designed with the aim to test circuital solution with other kind of harvesting sources and WSN nodes for expanding its potential applications; in this regard some selection jumpers are used to set, even after PCB realization, the DC output voltage value and UVLO thresholds. Each jumper allows to set corresponding selecting pin to low or high logic state according to WSN node features and energy harvesting source to be exploited. Aim is to minimize, as much as possible, backup batteries use by using solar cells energy when

available but also storing solar energy in super-capacitors in time periods of high energy availability and then providing it to feed node when no harvestable energy is available. Realized board has an input section for solar cells connection and output section for node power supply. Some connectors were placed on board in order to make circuit rearrangements and to increase device capabilities even after PCB realization. Figure 26 shows realized PCB layout by using CAD software Eagle: the PCB is composed by two layers (top and bottom).

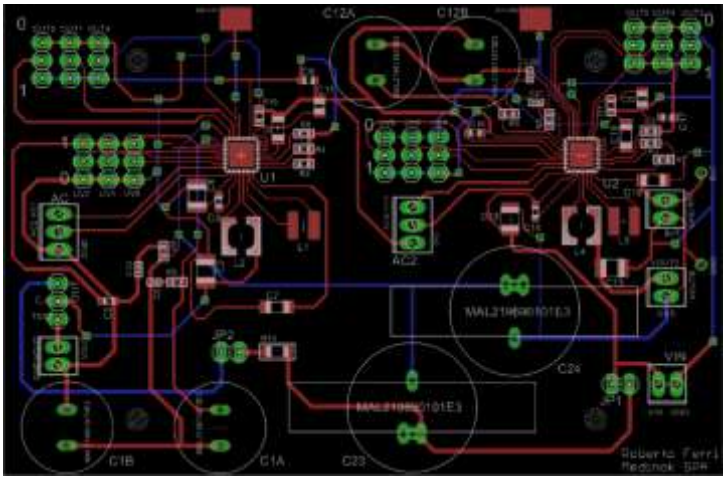


Figure 26. PCB layout of harvesting board for Medimote or low-power sensor node

On the PCB, three jumpers are also placed: jumper OUT is arranged to accept two different positions to connect the first LTC3330 stage to remaining part of the circuit otherwise to characterize only input stage decoupling it from the other blocks. Jumpers JP1 and JP2 have the task to decouple the three main blocks constituting the entire system. These jumpers are fundamental during PCB testing phase: in fact possible errors or problems can be easily found by examining separately each block. For possible future developments of proposed harvesting board, AC1 and AC2 inputs of the second block could be exploited to connect a second type of harvester creating a hybrid device able to accept more types of energy harvesting sources.

Figure 27 shows the realized PCB with pointed out the different sections: before connect the supercapacitors to PCB, some tests varying their nominal values were conducted to reduce the discharge slope of supercapacitors voltage. For verifying correct behavior of realized board, it was decided to use a DC power supply at the PCB input and to monitor Vout voltage across supercapacitors and the EH_{ON} pin voltage; in figure 28, the used experimental setup is shown.

In figure 29, the time function trends of voltages captured by the oscilloscope are shown. The behavior of the harvesting board in terms of UVLO rising and falling thresholds is correct: the prioritizer of the second LTC3330 IC decides to feed the sensor node by using energy stored in the supercapacitors when Vscap voltage across them exceeds the UVLO rising threshold.



Figure 27. Principal sections of harvesting board for Medimote power supply

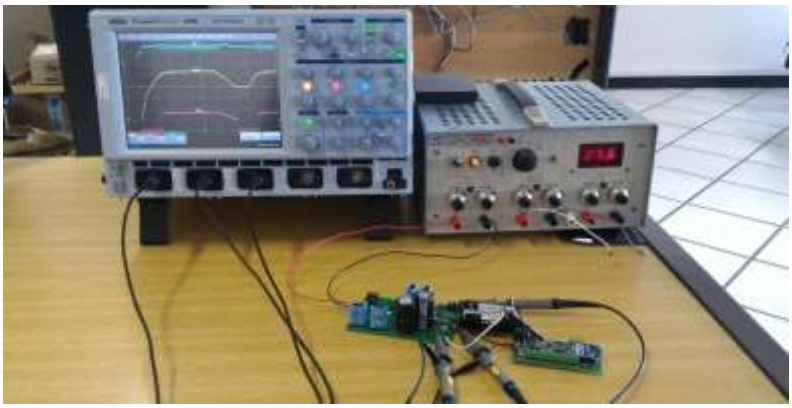


Figure 28. Experimental setup for electrical testing of the harvesting system operation

EH_{ON} logic level becomes high when supercapacitors voltage reaches 4V; if no harvestable energy is available or it isn't enough to feed WSN node, Vscap voltage starts discharge until it reaches 3V (UVLO falling threshold) under which *Medimote* is powered using backup battery.

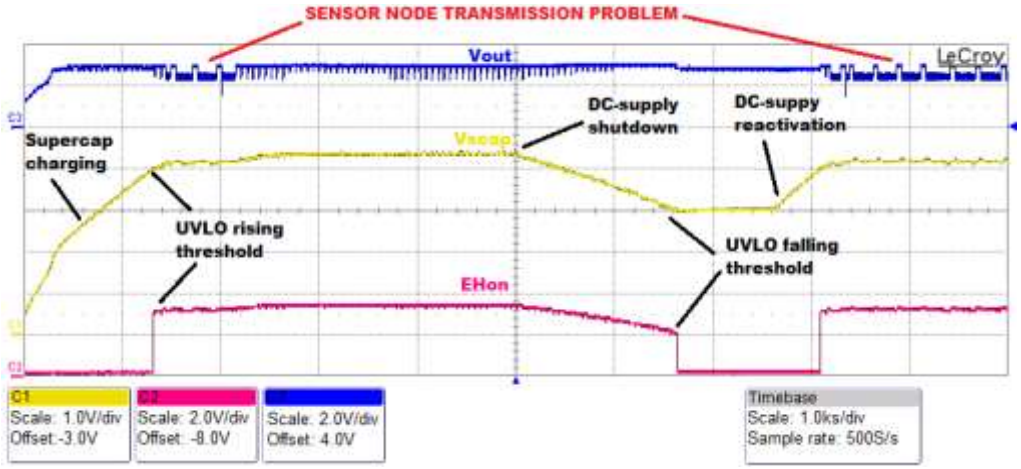


Figure 29. Output voltage measured before *Medimote* (blue colour), supercapacitor voltage (yellow) during normal functioning and shutdown and in purple, the EHON voltage trace.

By carrying out this test, a problem was found: the output voltage of second stage LTC3330 DC/DC converter was not fixed to 3V (node operating voltage) but presented significant voltage drops (hundreds of mV) during node transmission phase, but only if *Medimote* node was fed by energy stored in the supercapacitors. The identified transmission problem did not show up in the prototype discussed in the previous section and for this reason, wrong functioning's cause was attributed to a PCB error (wrong connection or sizing track, something that disagreed with guidelines outlined in the components' datasheet). After several tests carried out on the harvesting board, error was attributed to a not correct connection of GND exposed pad of the second stage; in fact, the GND pad of LTC3330 IC should be soldered to PCB ground using the lowest impedance path possible. After making the described circuital modification, the voltage drop, which occurs when node becomes active, was greatly reduced (only few mV), as shown in figure 30b.

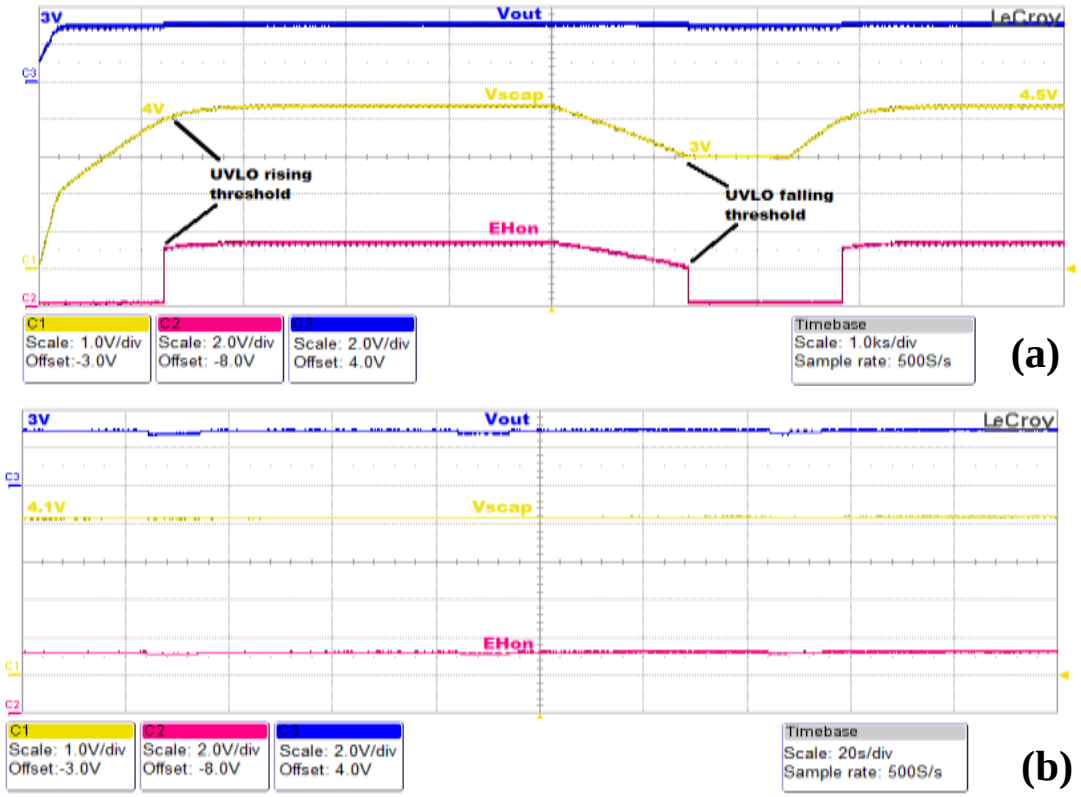


Figure 30. Transmission problem solved: output voltage in blue, supercapacitors voltage in yellow and in purple EHON voltage (a) and a zoomed view of transmission voltage drops (b).

As shown in figure 30a, the discharge time of supercapacitors, in absence of solar harvestable energy and using a total capacitance (C_{TOT}) value of 15F, is about 25 minutes, coherently with results obtained with demo-circuits based prototype. Super-capacitors charging phase up to 4V, when system is connected to the solar cells, lasts few minutes even with non-optimal lighting conditions. The goal is to decrease, as much as possible, the slope of supercapacitors

discharge phase in order to maximize the energy autonomy in absence of harvestable energy, so minimizing the use of backup batteries the sensor node is equipped with. For the following tests, capacitors of 30F and 100F were used in order to obtain respectively equivalent capacitance values of 15F, 50F and 100F exploiting series and parallel connections.

These experimental tests can be carried out having already verified that, when solar cells are used during daytime and eventually also in critical weather condition, the harvestable power is greater than that required for node functioning: supercapacitors can be easily charged up to 4.5V. Using the experimental setup shown in figure 31, it is possible to exactly monitor the voltage across supercapacitors before and during the discharge phase.

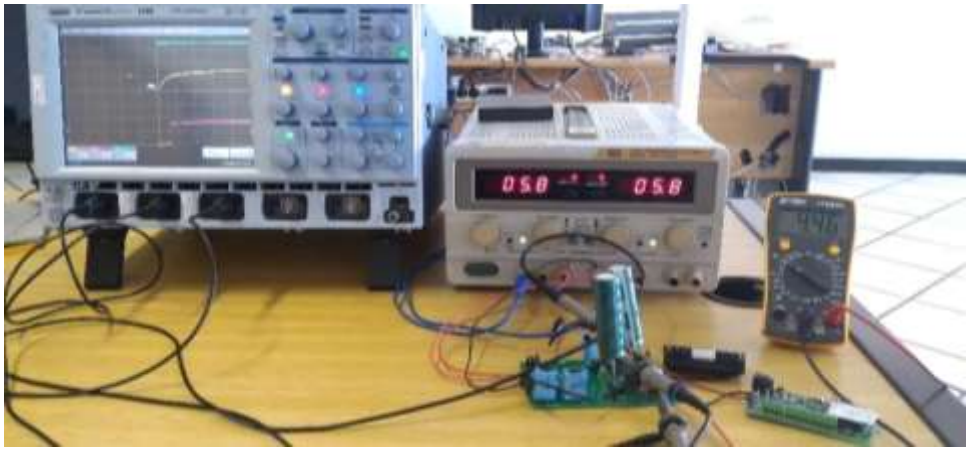


Figure 31. Experimental setup to monitor the supercapacitors voltage during discharge phase

The aim is determine the autonomy time, when no harvestable energy is available, for different supercapacitors values, measuring the discharge time during the transition of voltage across supercapacitors from 4.5V to 3V. Figure 32 shows how an increment of supercapacitors value leads to an increase of time required to discharge C_{TOT} from 4.5V to 3V. Previously, the discharge phase for a total capacitance C_{TOT} of 15F was shown; *Medimote* autonomy, when no harvestable energy is available from solar cells, was equal to 25min. By performing the same analysis, using C_{TOT} equal to 50F and 100F, a significant increase of the node power supply autonomy was obtained. With C_{TOT} = 50F, a discharge time of more than one hour (exactly 75 min) has been measured (as reported in figure 32a), before the prioritizer of the second LTC3330 stage decides to activate the backup batteries; instead, using a C_{TOT} equal to 100F, the discharge time amounts to two hours and half (as shown in figure 32b).

For the latest version of Medimote node, the absorbed current values during activity and sleep phases can be used to derive node power consumption for a single operating cycle: during data transmission phase, node requires 59mA while only about 7mA during the sleep phase.

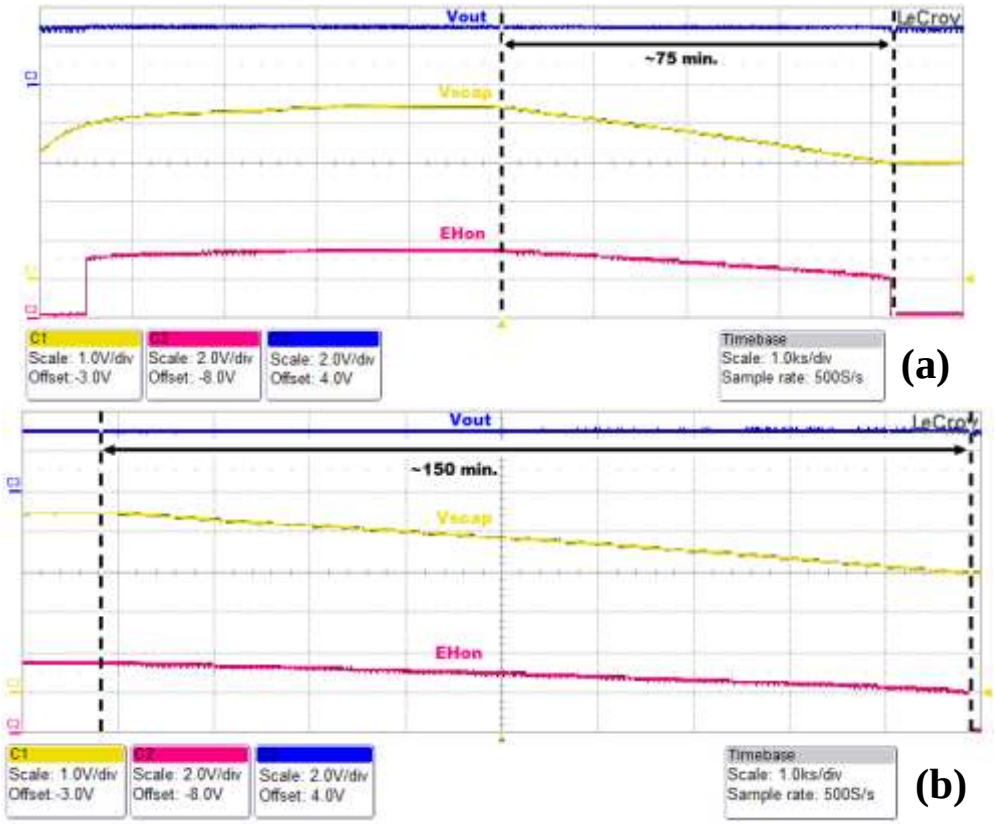


Figure 32. Capacitors discharge from 4.5V to 3V for CTOT equal to 50F (a) and 100F (b).

It is possible to derive the average current absorbed by *Medimote* during each operation cycle:

$$I_{single-cycle} = \frac{I_{max} \cdot 10 + I_{min} \cdot 50}{60} = \frac{59 \cdot 10^{-3} \cdot 10 + 7 \cdot 10^{-3} \cdot 50}{60} = 15.6mA$$

$$C_{TOT} = I_{single-cycle} \cdot \frac{\Delta t}{\Delta V_{single-cycle}}$$

Reversing the second relationship, voltage drop ΔV across supercapacitors that occurs for a single activity/sleep cycle is obtained. After, knowing the total variation of super-capacitors voltage during the discharge phase (ΔV_{TOT} = 4.5V – 3V) = 1.5V, the number of sensor node operating cycles that are guaranteed, before to involve the backup batteries, can be calculated. For CTOT values of 15F, 50F and 100F, therefore the following analyses can be carried out:

$$\Delta V_{single-cycle(15F)} = I_{single-cycle} \cdot \frac{t_2 - t_1}{C_{total}} = 15.6 \cdot 10^{-3} \cdot \frac{60}{15} = 62.4mV$$

$$\Delta V_{single-cycle(50F)} = I_{single-cycle} \cdot \frac{t_2 - t_1}{C_{total}} = 15.6 \cdot 10^{-3} \cdot \frac{60}{50} = 18.72mV$$

$$\Delta V_{single-cycle(100F)} = I_{single-cycle} \cdot \frac{t_2 - t_1}{C_{total}} = 15.6 \cdot 10^{-3} \cdot \frac{60}{100} = 9.36mV$$

Assuming that supercapacitors are fully charged to 4.5V, as confirmed by experimental tests, it is possible to calculate operating-cycles number relative to harvesting system's autonomy.

$$Operating - cycle_{15F} = \frac{\Delta V_{discharge-range}}{\Delta V_{single-cycle}} = \frac{4.5 - 3.0}{62.4 \cdot 10^{-3}} \simeq 24\ cycles$$

$$Operating - cycle_{50F} = \frac{\Delta V_{discharge-range}}{\Delta V_{single-cycle}} = \frac{4.5 - 3.0}{18.72 \cdot 10^{-3}} \simeq 80\ cycles$$

$$Operating - cycle_{100F} = \frac{\Delta V_{discharge-range}}{\Delta V_{single-cycle}} = \frac{4.5 - 3.0}{9.36 \cdot 10^{-3}} \simeq 160\ cycles$$

where $V_{discharge-range}$ is the total variation of supercapacitors voltage in the discharge phase (starting from about 4.5V until UVLO falling threshold - 3V - of second LTC3330 stage). In table 2, the comparison between number of autonomy cycles, mathematically and experimentally obtained, are reported.

Number of operative cycles		
Total Capacitance	**Mathematical Analysis**	**Experimental Analysis**
15F	24 cycles	25 cycles
50F	80 cycles	75 cycles
100F	160 cycles	150 cycles

Table 2. Number of autonomy cycles mathematically and experimentally obtained by varying the total capacitance value CTOT in complete absence of harvestable energy.

According to table 2, number of operative cycles experimentally determined that *Medimote* node can perform before supercapacitors voltage reaches the UVLO falling threshold (3V), in condition of harvestable energy absent, carefully follows the number of operative cycles calculated mathematically. By exploiting waveform data and corresponding CSV file obtained by the oscilloscope, an analysis related to a few operating cycles was carried out; in figure 33, the supercapacitors voltage detected by oscilloscope during the discharge phase and absence of harvestable energy, with CTOT equal to 50F is shown for only 15 operative cycles (900sec).

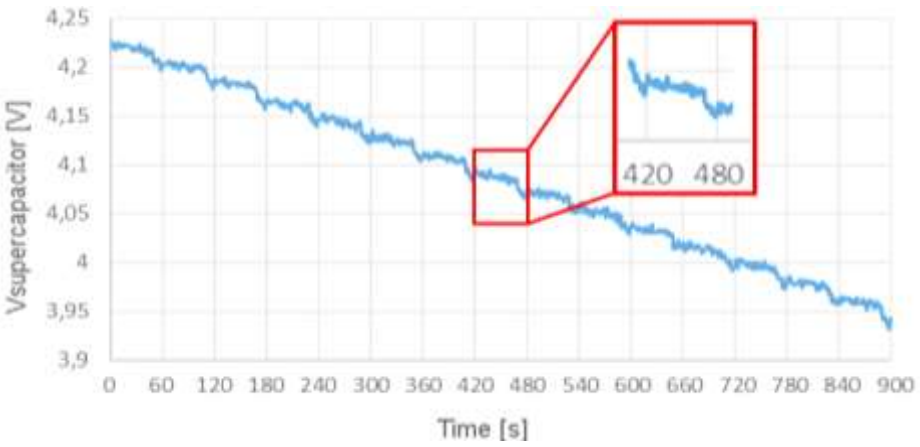


Figure 33. Detailed analysis of supercapacitors voltage discharge with CTOT equal to 50F.

As evident in the zoomed area, voltage decreases faster when the sensor node is active (data transmission phase for 10sec) and a high current is required; instead, voltage decreases slower when *Medimote* node is in sleep mode (for a time duration of 50sec). It has been demonstrated that for CTOT = 50F, a voltage drop of 18.72mV occurred for each operating cycle; it follows that for 15 operative cycles, the total voltage drop on the supercapacitors is equal to:

$$\Delta V_{15-cycles(50F)} = \Delta V_{single-cycle(50F)} \times 15 = 18.72 \cdot 10^{-3} \times 15 = 280.8mV$$

From figure 33, voltage across supercapacitors for 15 operative cycles and CTOT = 50F decreases from 4.22V up to 3.94V; the difference ΔV is equal to 280mV perfectly in agreement with mathematical analysis. In figure 34, 15 operative cycles (900sec) of the *Medimote* node have been monitored with CTOT value of 100F connected to the first LTC3330 stage output.

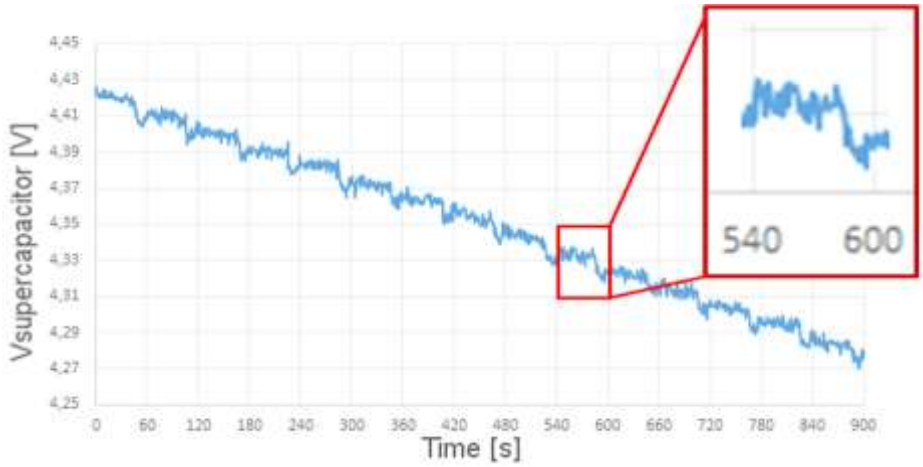


Figure 34. Detailed analysis of supercapacitors voltage discharge with CTOT equal to 100F.

It has been demonstrated that for CTOT = 100F, a voltage drop of 9.36mV occurred for each cycle; therefore after 15 operative cycles, total voltage drop on the supercapacitors is equal to:

$$\Delta V_{15-cycles(100F)} = \Delta V_{single-cycle(100F)} \times 15 = 9.36 \cdot 10^{-3} \times 15 = 140.4mV$$

According to figure 34, supercapacitors voltage for 15 operative cycles decreases from 4,42V up to 4,28V and thus the total voltage drop, experimentally obtained, is equal to 140mV, exactly the same value obtained by mathematical calculations. At last, a final verification of the harvesting board functioning using solar cells, as energy harvesting source, was carried out. The used experimental setup is shown in figure 35; graphs detected by oscilloscope and shown in figure 36 confirm the proper functioning of the realized and fully-tested harvesting system. The supercapacitors are charged up to 4.5V, the chosen output voltage of first LTC3330 stage. The use of higher CTOT values leads to longer charging time; despite this observation, many analyses varying CTOT value were carried out.

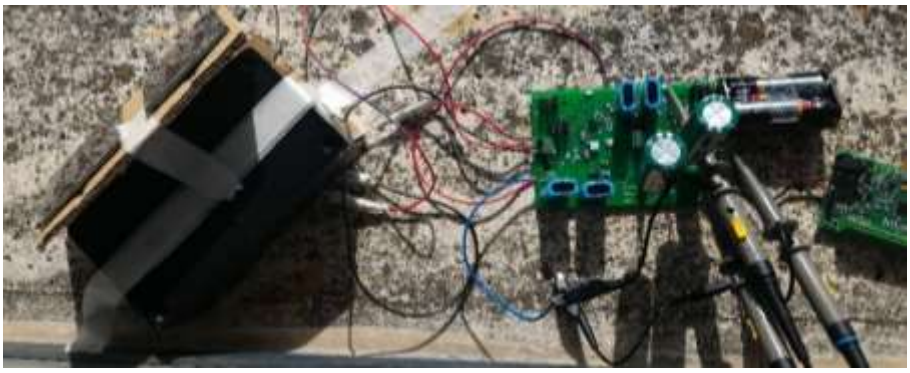


Figure 35. Experimental setup used for the final testing of realized harvesting system

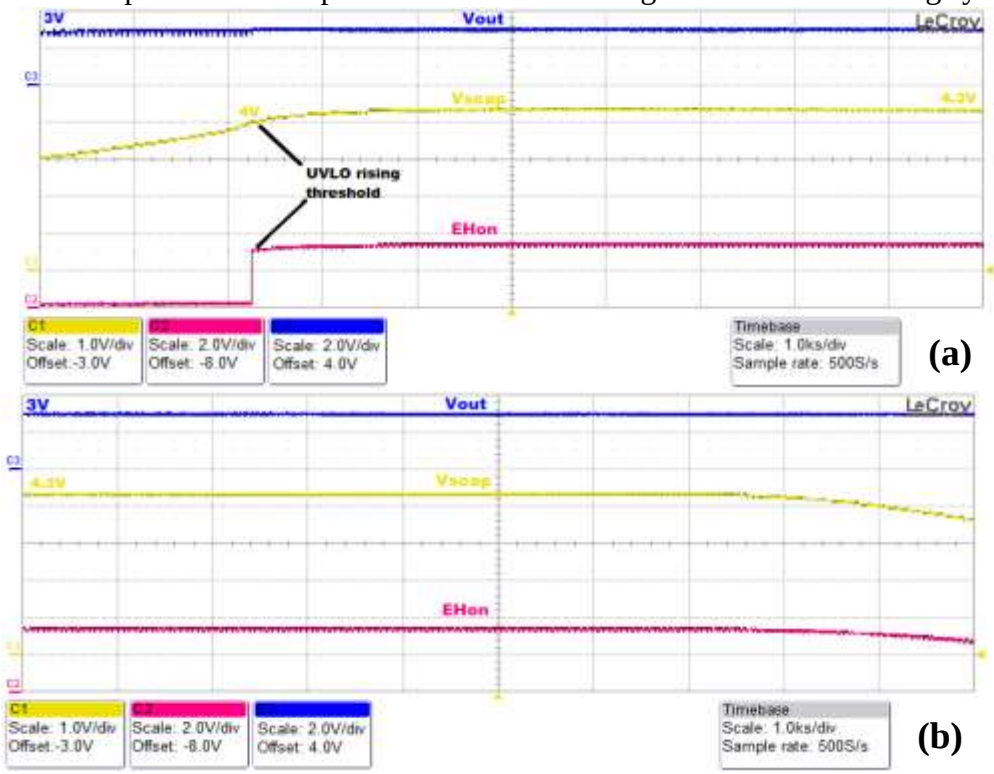


Figure 36. Final test of the harvesting board with averagely good condition (a) and in the evening proximity (b): with blue colour, the output voltage applied to the Medimote node, with yellow colour the supercapacitors voltage trace and with purple colour EH_{ON} trend.

The power supplied by solar cells, even in non-optimal lighting conditions is high enough and so supercapacitors charging phase is sufficiently fast; for this reason, the increase of C_{TOT} value for improving *Medimote* energy autonomy, without involving backup batteries, is a viable alternative. When solar cells are subject to lighting conditions that do not allow to derive sufficient energy, voltage across supercapacitors never reaches 4.5V. After passing UVLO rising threshold, prioritizer enables the harvester branch and supercapacitors provides energy to feed the sensor node. When solar cells are not able to provide sufficient energy to ensure node operation being power required by *Medimote* higher than the one harvestable, supercapacitors begin discharge phase with a slope that depends on the energetic balance.

VII. CONCLUSIONS

The developed harvesting board can be provided to many types of WSN node; depending on the scenario and kind of available energy, a harvester can be appropriately chosen in order to derive the energy from the environment to ensure sensor node operation. In figure 37, the final structure of the designed and realized harvesting board is shown; the device has two inputs, corresponding to AC1 and AC2 input pins of first LTC3330 stage and one output for sensor node connection. The developed system can be easily adapted to other application contexts and other WSN nodes: the energy source's inputs of realized harvesting board consists of an integrated full-wave bridge rectifier and a high voltage buck converter that allow to harvest energy not only from solar cells but also from piezoelectric, magnetic or electromagnetic sources and more in general, from alternative AC power sources. Inside the harvesting board package, a battery holder is available to easily insert the backup batteries.



Figure 37. Final structure of the developed harvesting board for WSN node power-supply.

Based on LTC3330 IC technical features, a complete circuit diagram for energy harvesting and power management has been designed, able to ensure the power supply of WSN node and optimal exploitation of available energy. In fact, the developed board allows to control and track the MPP of energy source connected as input, by exploiting the LTC3330 UVLO functionality. The proper functioning of the sensor node and the respective capabilities within the network are guaranteed under any condition of energy harvestable from the environment: the LTC3330 internal prioritizer carries out a control on the availability of harvestable energy and involves backup battery to ensure the proper operation of the sensor node when the source of harvesting is not available. The prioritizer, in fact, decides whenever to use the energy harvesting input or the battery input to ensure stable V_{OUT} for feeding the WSN node.

The proposed solution also guarantees supercapacitor charging when the harvestable energy is higher than the one required from the sensor node. This stored energy is then used in critical energy conditions obtainable from the harvester, before requesting the intervention of backup batteries. The carried out mathematical analyses allowed to link the consumption of the sensor node and the supercapacitors discharge voltage. Knowing the absorbed current value from a generic sensor node (in each phase of its operative cycle), it is possible to find the total capacitance value C_{TOT} that guarantees a given and desired energy autonomy (in terms of numbers of operative cycles) in absence of harvestable energy. The perfect agreement between the experimental observations and mathematical results has provided a basis for supercapacitor dimensioning and, in addition, validates the operation of the developed harvesting device. For future developments, particular prominence should be given to the AC input connector of the second LTC3330 stage that could be exploited in order to connect a second type of harvester creating a hybrid energy harvesting and power management solution.

REFERENCES

[1] J. Gubbi, R. Buyya, S. Marusic, M. Palaniswami: Internet of Things (IoT): A vision, architectural elements, and future directions. Future Generation Computer Systems, Vol. 29 (7), pp. 1645-1660 (2013).

[2] M. Weiser, R. Gold, J. S. Brown: The origins of ubiquitous computing research at PARC in the late 1980s. IBM Systems Journal, Vol. 38 (4), pp. 693-696 (1999).

[3] O. Vermesan, P. Friess. Book: Internet of Things: Converging Technologies for Smart Environments and Integrated Ecosystems. River Publishers series in Communications (2013).

[4] P. Visconti, A. Lay-Ekuakille, P. Primiceri, G. Cavalera: Wireless Energy Monitoring System of Photovoltaic Plants with Smart Anti-Theft solution integrated with Household Electrical Consumption's Control Unit Remotely Controlled by Internet. International Journal on Smart Sensing and Intelligent Systems, Vol. 9 (2), pp. 681 – 708 (2016).

[5] P.Primiceri, P.Visconti, A.Melpignano, A. Vilei. G.M. Colleoni: Hardware and software solution developed in ARM mbed environment for driving and controlling DC brushless motors based on ST X-NUCLEO development boards. International Journal on Smart Sensing and Intelligent Systems, Vol. 9 (3), pp. 1534 - 1562 (2016).

[6] G. Edwin Prem Kumar, K. Baskaran, R. Elijah Blessing, M. Lydia: A comprehensive review on the impact of compressed sensing in wireless sensor networks. International Journal on Smart Sensing and Intelligent Systems, Vol. 9 (2), pp. 818 – 844 (2016).

[7] Internet of Things: Wireless Sensor Network, White Paper – International Electrotechnical Commission, http://www.iec.ch/whitepaper/pdf/iecWP-internetofthings-LR-en.pdf .

[8] C. Y. Lin, S. Zeadally, T. S. Chen, C. Y. Chang: Enabling cyber physical systems with wireless sensor networking technologies. International Journal of Distributed Sensor Networks, Article ID 489794, 21 pages, DOI: 10.1155/2012/489794 Vol. 8 no. 5 (2012).

[9] B. Zhou, J. Cao, J. Li: An adaptive traffic light control scheme and its implementation in WSN-based its. International Journal on Smart Sensing and Intelligent Systems Vol. 6 (4), pp.1589-1881 (2013).

[10] Wireless Mesh Networking - ZigBee vs Digi-Mesh, White Paper http://www.digi.com/pdf/wp_zigbeevsdigimesh.pdf .

[11] J. S. Lee, Y. M. Wang: Experimental evaluation of Zig-Bee-based wireless networks in indoor environments. Journal of Engineering, Vol. 2013 - Article ID 286367, 9 pages http://dx.doi.org/10.1155/2013/286367 (2013).

[12] G. Anastasi, M. Conti, M. Di Francesco: Extending the lifetime of wireless sensor networks through adaptive sleep. IEEE Transactions on Industrial Informatics, Vol. 5 (3), pp. 351-365 (2009).

[13] J. M. Gilbert, F. Balouchi: Comparison of energy harvesting systems for wireless sensor networks. International Journal of automation and computing, Vol. 5 (4), pp. 334-347 (2008).

[14] M.Bellevile, E.Cantatore, P. Fiorini, P. Nicole, M. Pelgrom, C. Piguet, C.Vullers, M.Tartagni: Energy Autonomous Systems: Future Trends in devices technology and Systems. Cluster for Application and Technology Research in Europe on Nanoelectronic (2009).

[15] G. Zhou, L. Huang, W. Li, Z. Zhu: Harvesting ambient environmental energy for wireless sensor networks: a survey. Journal of Sensors, Vol. 2014, Article ID 815467, 20 pages, http://dx.doi.org/10.1155/2014/815467 (2014).

[16] R. J. M. Vullers, R. Van Schaijk, I. Doms, C. Van Hoof, R. Mertens: Micropower energy harvesting. Solid-State Electronics, Vol. 53 (7), pp. 684-693 (2009).

[17] K. H. Chao, Y. H. Lee: A maximum power point tracker with automatic step size tuning scheme for photovoltaic systems. International Journal of Photoenergy, Vol. 2012, Article ID 176341, 10 pages, http://dx.doi.org/10.1155/2012/176341 (2012).

[18] R. Hemalatha, R. Ramaprabha, S. Radha: A comprehensive analysis on sizing of solar energy harvester elements for wireless sensor motes. International Journal on Smart Sensing and Intelligent Systems, Vol. 8 (1), pp. 291-315 (2015).